PAPER

Check for updates

Stacked meshes with super-wettability *via* atmospheric plasma for efficient emulsion separation†

Zengyi He,[a,b] Linfeng Yang,[a,b] Xinpeng Cao,[a,b] Shan Zhou,[a] Lei Jiang [ID] [a,b] and Haoyu Dai [ID] *[a,b]

Common filter membranes for emulsion separation often require time-intensive preparation and extensive use of chemicals, necessitating a fast-processing and eco-friendly alternative. This study introduces a 2-layer stacked nylon mesh treated with surface diffuse atmospheric plasma (SDAP) for rapid and efficient emulsion separation. Commercial nylon mesh exhibited durable super-wetting properties after just 30 s of SDAP treatment, which was sufficient for effective emulsion separation. Multi-layer stacking further enhanced the oil-blocking capacity, with pre-wetted 2-layer meshes achieving over 98% separation efficiency, a flux exceeding 56 000 L m^{-2} h^{-1} bar^{-1} and excellent anti-aging performance, demonstrating applicability across various emulsions simultaneously. The emulsion droplet dynamics within the filter cake revealed high efficiency, offering valuable insights into membrane fouling issues. Furthermore, this work develops SDAP as a promising approach for material treatment, owing to its fast and environmentally friendly processing, scalable set-up and effectiveness under atmospheric conditions.

[a]CAS Key Laboratory of Bio-inspired Materials and Interface Sciences, Technical Institute of Physics and Chemistry, Chinese Academy of Sciences, Beijing 100190, China. E-mail: daihaoyu@mail.ipc.ac.cn
[b]School of Future Technology, University of Chinese Academy of Sciences, Beijing 100049, China
†Electronic supplementary information (ESI) available. See DOI: https://doi.org/10.1039/d4nr04457f

Haoyu Dai is currently an Associate Professor at the Technical Institute of Physics and Chemistry, Chinese Academy of Sciences. He received his B.Sc. degree (2015) from Tsinghua University and his PhD (2020) from Peking University, where he was supervised by Prof. Lei Jiang. His research interests focus on liquid dynamics at interfaces with super-wettability, including the development of super-wetting materials, electrically controlled liquid transport, and plasma-induced surface functionalization, with a focus on their industrial applications.

Haoyu Dai

Introduction

The expansion of global oil trade has led to inevitable natural leaks during transportation, coupled with human-induced emissions from ships and land-based activities, making oil pollution a major environmental concern worldwide.[1] In the face of such problems, extensive research efforts have been directed toward efficiently separating oil–water mixtures over the past few decades.[2–6] However, emulsions, which are common pollutants following oil spills, present a greater challenge due to the presence of surfactants that disperse oil droplets into water at the micro/nanoscale. This is especially problematic for the effective separation of oil–water mixtures in stable oil-in-water (O/W) emulsion systems using conventional methods.[7,8] Therefore, the rapid and efficient destabilization of emulsions for effective emulsion separation has emerged as a critical scientific challenge.

In recent years, substantial progress has been made in emulsion separation methods, such as particle adsorption, chemical demulsification, and membrane separation.[4,9,10] Innovative approaches, including the use of corona discharge to generate charged active particles for breaking O/W emulsions and the dual bionic super-wetting gear inspired by hogweed, have also shown reliability.[11,12] Among these techniques, membrane separation technology is particularly promising due to its merits, such as high water quality, energy efficiency, and the absence of phase transitions, especially

when applied to super-wetting membranes.[13] By tuning the surface chemistry and micro/nanoscale structure, membranes can exhibit superhydrophobicity and superoleophilicity, or superhydrophilicity and underwater superoleophobicity, making them highly effective for emulsion separation.[14] Although various super-wetting membranes, including metal–organic framework (MOF) stencil membranes,[15,16] graphene membranes,[17,18] polyvinylidene fluoride (PVDF) membranes,[19,20] and nanofiber membranes,[21,22] have been successfully used for emulsion separation, challenges such as slow synthesis, difficult recovery, and low flux remain significant barriers to their widespread application. As a result, there is an urgent need for fast, environmentally friendly, and scalable methods for producing super-wetting membranes.

In nature, many surfaces exhibit super-wettability. For instance, fish scales achieve underwater superoleophobicity through their micro/nanoscale structures.[12,23,24] Inspired by these natural systems, constructing micro/nanoscale structures on existing membranes or meshes offers a fast and effective approach to create super-wetting materials for emulsion separation. Among the common methods for material surface etching and hydrophilization, plasma treatment is a simple and rapid technology that involves little or no use of chemical reagents.[25] Plasma etching creates micro/nanoscale structures on material surfaces while high-energy active particles simultaneously graft onto the surface, inducing a synergistic effect that results in hydrophilicity and underwater oleophobicity.[26] Compared with vacuum plasma, which requires strict conditions, commonly used atmospheric plasma, such as atmospheric plasma jets and inert gas plasma, represents a major technological advancement.[27–29] However, with the increasing focus on atmospheric plasma for surface wettability modification, relevant limitations, including confined treatment areas and the need for inert gas environments, have become more apparent.[30] As an emerging type of plasma generated by coplanar dielectric barrier discharge (CDBD), surface diffuse atmospheric plasma (SDAP) allows direct surface modification under atmospheric conditions without the demand for an inert gas atmosphere.[31] Due to its flexible discharge region, ultra-high energy density, and low-temperature characteristics, SDAP shows considerable potential in various applications, particularly for those requiring rapid, continuous, and large-scale hydrophilization of material surfaces.[32] Previous studies have also demonstrated that SDAP-treated nylon mesh enables efficient large-area oil/water separation, offering high separation efficiency, water flux, and broad applicability.[31]

In this study, we demonstrate that a nylon mesh treated with SDAP within 2 s achieves hydrophilicity and underwater oleophobicity. By stacking multiple layers, the effective pore size of the treated meshes is significantly reduced, enabling high separation efficiency in O/W emulsion separation. The tightly stacked nylon meshes achieve a smaller effective pore size in the lateral cross-section and form a complex 3-dimensional structure in the vertical direction, which is an advantage that is challenging to replicate with 1-layer membranes or multi-stage filtration, even if the 1-layer membranes may have

smaller pore sizes. This combination of structural benefits markedly enhances both the separation efficiency and stability, with interlayer permeation partially substituting for vertical permeation. Notably, compared to previous studies, this study further broadens the application scope of SDAP.[31,33,34] Unlike the simple mechanism of oil–water separation achieved with a single-layer nylon mesh, the observation of the filter cake in this study provides deeper insights into the dynamics of emulsion droplets within it. This not only helps elucidate the mechanism behind efficient emulsion separation but also offers more complex and valuable references for research on membrane fouling. In addition, the treated meshes exhibit excellent anti-aging properties, cycling durability, and pressure resistance. Overall, the SDAP-treated 2-layer stacked nylon meshes demonstrate excellent emulsion separation performance for a wide range of O/W emulsions formulated with different oils and surfactants, offering advantages such as rapid treatment, secondary pollution free, and suitability for large-scale applications, opening an avenue for future technology on environmentally friendly dealing with fouling issues.

Results and discussion

Achieving super-wettability on nylon mesh by SDAP

The process of surface diffuse atmospheric plasma (SDAP) treatment of nylon mesh and a schematic diagram of the changes before and after modification are shown in Fig. 1a. The original nylon mesh does not exhibit any special superwetting properties, whether in air or water. Once treated with SDAP, the nylon mesh changes from a water contact angle of $107° \pm 0.9°$ in the air to a superhydrophilic state. Meanwhile, the oil contact angle changes from the original $81.3° \pm 8.6°$ to an oleophobic state with an angle of $147.9° \pm 0.8°$. It is acknowledged that filter membrane materials, which are superhydrophilic and underwater oleophobic, can be applied for emulsion separation.[24] Additionally, the fiber transformation diagram in Fig. 1a illustrates the significant wettability transition of the nylon mesh induced by SDAP treatment. This transition occurs because the oxygen-rich atmosphere generates plasma under a high-frequency alternating electric field that continuously bombards the surface of the nylon fibers, resulting in enhanced roughness while simultaneously grafting oxygen-containing functional groups onto the nylon surface. This dual action effectively promotes the modification of the nylon meshes with super-wettability.

Fig. 1b illustrates the schematic of the experimental set-up for emulsion separation with SDAP-treated multi-layer nylon meshes. The process flow for separation and optical micrographs of emulsions before and after separation is shown in Fig. 1c. In the separation process, the SDAP-treated multi-layer nylon meshes are pre-wetted with water and fixed between two inner tubes. When the well-dispersed O/W emulsion is poured into the upper tube, the water-coated meshes block the oil droplets but allow water to pass through. As shown in the final stage of the separation in Fig. 1c, as the water content in the
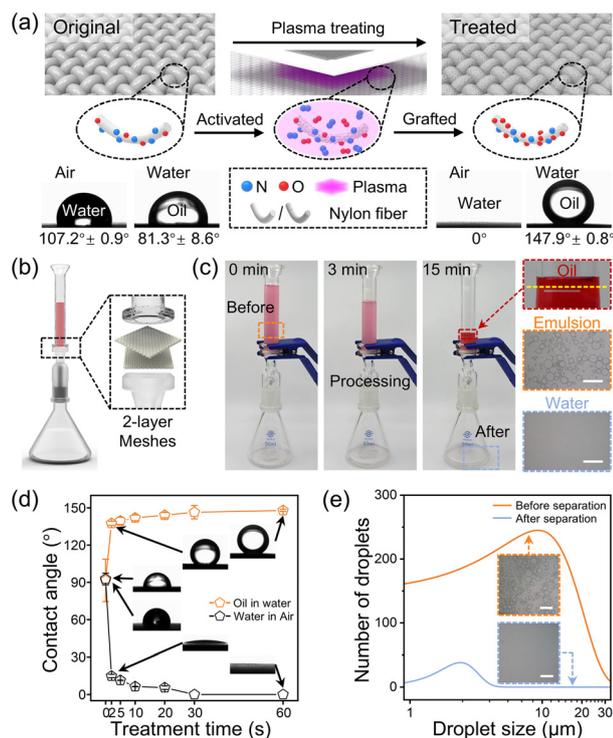
Fig. 1 Demonstration of nylon mesh treated with plasma and further application in emulsion separation. (a) Schematic of the process of nylon mesh treated by surface diffuse atmospheric plasma (SDAP). Insets are the images of water contact angle and underwater oil contact angle of the original and treated nylon mesh, respectively. (b) Schematic of the emulsion separation set-up with 2-layer SDAP-treated nylon meshes stacked at a 45° angle. (c) Optical images of the emulsion separation process. Upper right inset shows the free oil separated from the emulsion. Middle and lower right insets are the microscopic images of the emulsion before and after separation, respectively. Scale bar, 100 μm. (d) Water contact angle and underwater oil contact angle of nylon mesh with different SDAP treatment time. (e) Statistical distribution of droplet sizes in the emulsion before and after separation by 2-layer stacked SDAP-treated nylon meshes. Insets are the microscopic images of the emulsion before (9.27 ± 0.79 μm) and after (2.44 ± 0.13 μm) separation, respectively. Scale bar, 100 μm.

upper tube decreases, trapped droplets coalesce into larger droplets and eventually form a free oil layer on the emulsion surface, leading to the oil/water phase separation. In a securely mounted state, the surface tension of water and the adhesive forces of the filter cake collectively ensure a strong bond between the upper and lower layers of the nylon mesh. At an input power of 100 W, the relationship between SDAP treatment time and the water contact angle in air and oil contact angle in water of nylon mesh is presented in Fig. 1e. Due to the extremely high surface energy density and low energy dissipation resulting from the low thickness of the SDAP,[32] even with a treatment time of 2 s, the hydrophilicity and underwater oleophobicity of the nylon mesh are greatly enhanced. Within 30 s, the nylon mesh achieves super-wettability suitable for emulsion separation, showing rapid water spreading in the air and minimal underwater oil adhesion (Fig. S1†). Even for emulsions with droplets smaller than 10 μm, the SDAP-treated

2-layer nylon meshes show excellent separation efficiency, as observed in the optical micrographs and droplet size distribution in Fig. 1e and Fig. S2.†

Surface morphology and chemical characterization

To investigate the fundamental mechanism behind the wettability changes in SDAP-treated nylon mesh, characterizations including optical microscope, scanning electron microscope (SEM), atomic force microscope (AFM), and X-ray photoelectron spectroscopy (XPS) were performed. Fig. 2a and b show the optical and microscope photographs of the nylon mesh before and after treatment, demonstrating that the nylon mesh treated with 30 s SDAP does not exhibit significant material damage. On the one hand, the single-surface uniform discharge of SDAP effectively prevents arc damage caused by local breakdown; on the other hand, the low-temperature characteristic of SDAP protects the treated material from high-temperature damage.[35] The optical photograph of the SDAP system used in this study is shown in Fig. S3.† The plasma generation mechanism is based on the CDBD mechanism, with a plasma layer thickness of approximately 0.3 mm. Besides, SDAP forms a uniformly diffused plasma that consists of many independent filamentary discharge paths between the electrodes on the surface of a single-side dielectric. Infrared imaging measurements indicate that, at an input power of 100 W, the macroscopic temperature of the surface-diffusion atmospheric plasma does not exceed 82.22 °C, which proves that it is a low-temperature treatment technology suitable for treating nylon mesh (Fig. S4†). Fig. 2c and d show the SEM images of nylon mesh before and after SDAP treatment under different magnifications. It can be confirmed that the untreated nylon mesh surface is relatively smooth, with only streamlined traces formed during the polymer fiber extrusion process. In contrast, the surface morphology of the nylon mesh treated with SDAP for 60 s shows micro/nanoscale papilla structures, along with larger particulate deposits. These changes can be attributed to the etching effect of SDAP on the nylon fiber surface. The bombardment of high-energy particles causes the cleavage of certain chemical bonds, facilitating the grafting of more oxygen-containing functional groups. Concurrently, the small fragments detached from the fiber are either expelled into the atmosphere through thermal convection or deposited in other areas on the nylon surface. Ultimately, this process results in a nylon mesh with increased oxygen content and enhanced surface roughness. Fig. 2e and f further confirm the increased roughness of the nylon fibers after SDAP treatment through AFM images. The cross-sectional profile of the original nylon fibers maintains a certain curvature, while the SDAP-treated nylon fibers exhibit an irregular papilla appearance. As the SDAP treatment time increases from 0 to 60 s, the roughness of nylon fiber significantly increases from the original 7.3 nm to 44.7 nm (Fig. S5†).

Overall, SDAP is generated in an oxygen-rich atmospheric environment, which subsequently leads to the grafting of oxygen elements from the atmosphere onto the nylon fiber surface *via* plasma. This is confirmed by the XPS analysis
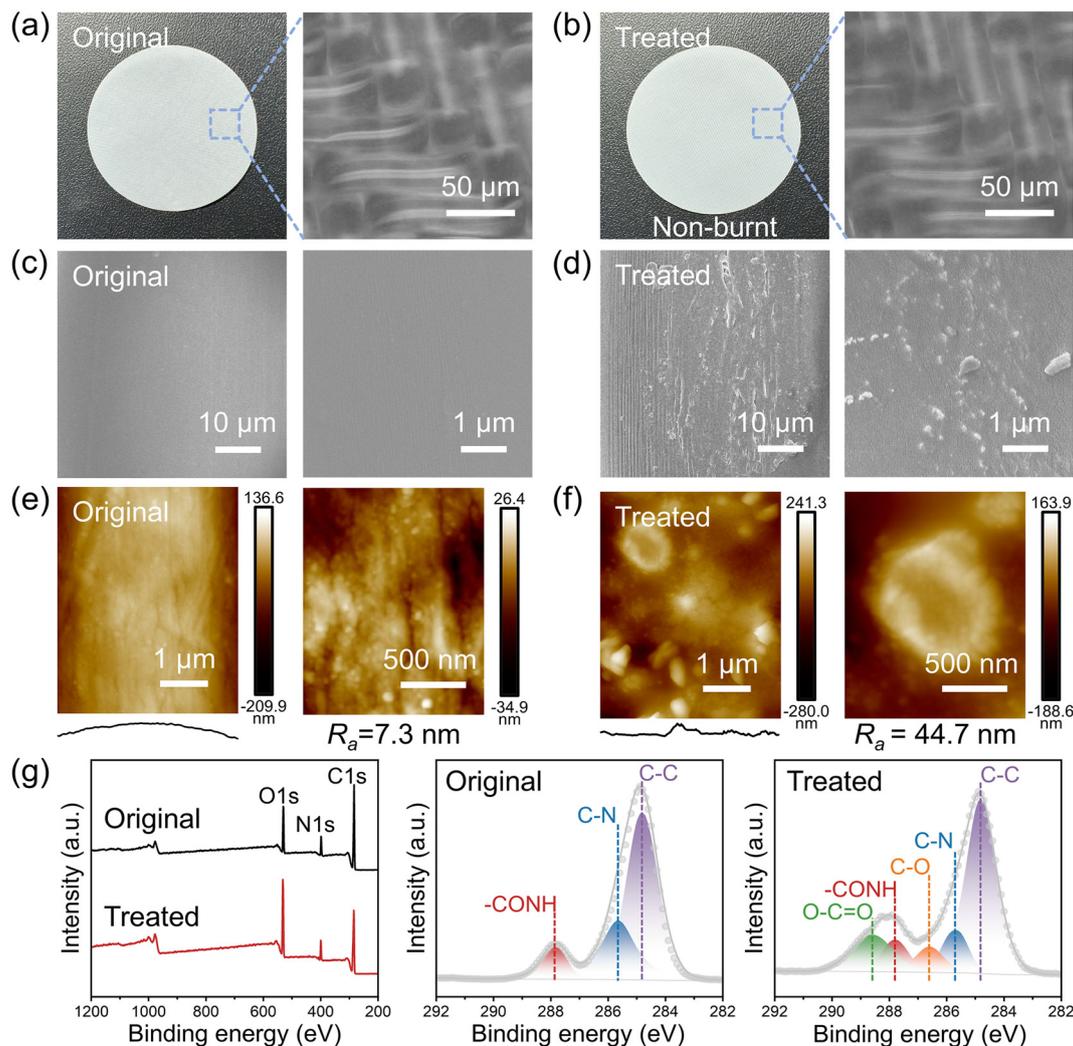
Fig. 2 Surface characteristics of nylon mesh before and after SDAP treatment. (a) and (b) Optical and microscopic images of original and treated nylon mesh. (c) and (d) Scanning electron microscope (SEM) images of original and treated nylon mesh exhibit distinct micro-nanoscale structures on the material surface after SDAP treatment. (e) and (f) Atomic force microscope (AFM) images of original and treated nylon meshes demonstrate that the surface roughness significantly increases, with the cross-sectional profile changing from a regular curvature to an irregular appearance. (g) X-ray photoelectron spectroscopy (XPS) spectra and peak-fitted high-resolution C 1s spectra of original and treated nylon meshes demonstrate oxygen-containing species increased after SDAP treatment.

shown in Fig. 2g, which provides insight into the chemical composition of the surface. The relative contents of C, N, and O before and after treatment are recorded in Table 1. Polyamide 66, the primary component of the nylon mesh, contains only C, N, and O, and the relative contents of these elements in the untreated nylon mesh were 74.10%, 9.99%, and 15.92%, respectively, while after treatment, the contents were 63.62%, 10.15%, and 26.23%, respectively, with the oxygen content increasing by 10.31%. High-resolution XPS analysis of the C 1s peak further elucidates the changes in functional groups on the nylon surface before and after treatment. The analysis result indicates that SDAP treatment introduces more oxygen-containing functional groups, such as C–O and O–C=O. Furthermore, under the continuous bombardment of high-energy particles in the plasma, surface chemical

bonds in the polymer undergo continuous cleavage and subsequently form oxygen-containing polar functional groups, such as –OH and –COOH, with abundant oxygen radicals in the plasma. This results in an increase in oxygen content. The high-resolution peak fitting of the O 1s XPS (Fig. S6†) confirms the formation of new O–C bonds after treatment. Moreover, the high-resolution N 1s peak fitting XPS (Fig. S7†) reveals the appearance of peaks representing high-valence nitrogen species after the SDAP treatment of the nylon mesh. These radicals interact with active species in the plasma, further increasing the oxygen content. Overall, the combined effect of the micro/nanoscale structure formation and the increase in oxygen-rich polar functional groups transform the SDAP-treated nylon mesh into a superhydrophilic state.

Table 1 Relative contents of the elements and deconvolution analysis of C 1s peaks of the original and SDAP-treated nylon meshes

	Original (at %)	Treated (at %)		Original (at %)	Treated (at %)
C 1s	74.10	63.62	C–C	59.61	57.02
N 1s	9.99	10.15	C–N	29.86	11.39
O 1s	15.92	26.23	–CONH	10.53	8.66
			C–O	0	7.67
			O–C=O	0	15.26

Emulsion separation performance and mechanism analysis

In previous studies, SDAP-treated nylon mesh was proven to efficiently separate oil/water mixtures.[31] However, emulsion separation is more difficult than oil/water separation. Oil/water separation merely requires the nylon mesh pore size to meet the intrusion pressure requirements of the oil phase, while emulsion separation requires the pore size to be sufficiently small to block tiny emulsified oil droplets. For the nylon mesh applied in this study, multi-layer stacking is the fastest and simplest method to reduce the effective pore size. Fig. 3a illustrates the relationship between the number of stacked layers and the effective pore size. 600# nylon meshes were chosen as the model and experimental object, and the average effective pore size of the stacked layers was calculated using CAD software. The stacking principle was uniform: for two layers, adjacent nylon meshes were staggered by 45°, and for three layers, they were staggered by 30°, as shown in Fig. S8.† The SEM image of a 2-layer stack of treated nylon mesh is also presented in Fig. 3a. The originally intact square pores of the upper mesh are divided into smaller pores by the fibers of the lower mesh, significantly reducing the effective pore size in the cross-sectional view, which greatly enhances the ability to block tiny emulsion droplets. Although the effective pore size appears to be 0 in the top-view perspective when 3 or more layers are stacked, the multilayer structure is not entirely gap-free. In a three-dimensional space, gaps remain between the layers, which allows for emulsion separation. Adjusting the staggered angle between 2-layer nylon meshes was not used as a variable because it requires accounting for varying weaving
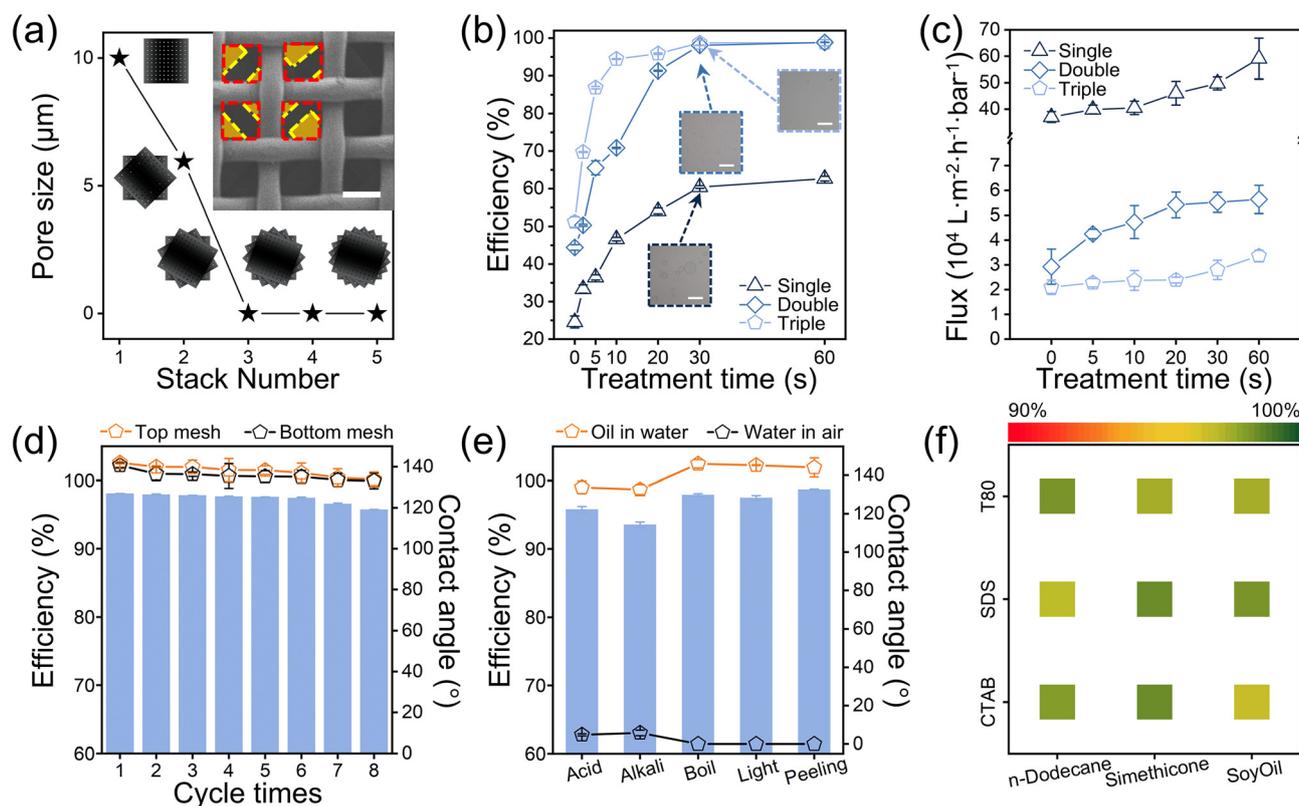
Fig. 3 Performance of multi-layer stacked nylon meshes in emulsion separation. (a) Equivalent pore size statistics for meshes with different stacking layers and corresponding stacking diagrams. The right top inset shows SEM image of 2-layer nylon meshes treated with SDAP, stacked at a 45° angle, in which red and yellow dotted lines indicate the upper and lower fibric boundaries, respectively, and the orange shaded area describes the effective filtration pore after stacking. Scale bar, 100 μm. (b) and (c) Separation efficiency and flux of 1-layer, 2-layer, and 3-layer stacked nylon meshes with different treatment time. (d) Separation efficiency and underwater oil contact angle of the upper and lower nylon meshes at the end of each separation cycle (from 1 to 8) for 2-layer stacked nylon meshes treated by SDAP. (e) Separation efficiency, water contact angle and underwater oil contact angle of 2-layer nylon meshes treated with SDAP under the following conditions: acid (pH = 2 HCl, 24 h), alkali (pH = 12 KOH, 24 h), boil (90 °C water 10 min), light (365 nm ultraviolet light, 200 mW cm^{-2}, 5 min), and peeling (15 cycles of tape peeling). (f) Separation efficiency of 2-layer nylon meshes treated with SDAP for emulsions with different surfactants and oil content.

patterns and offers a limited impact on separation efficiency, as changes in transmission area by changes of angle are minimal and less effective compared to adjustments in SDAP treatment time or the number of stacked layers.

By varying the SDAP treatment time to test the emulsion separation efficiency with different stacking layers, the resulting relationship curves are presented in Fig. 3b. The separation efficiency η is given by eqn (1):

$$\eta = \frac{c_{\text{initial}} - c_{\text{final}}}{c_{\text{initial}}} \times 100\%, \tag{1}$$

where c_{initial} and c_{final} represent the initial and final concentrations of the emulsion, respectively. This formula quantifies the effectiveness of the separation process under varying conditions of SDAP treatment time and nylon mesh stacking layers. As shown in Fig. 3b, the increase in stacking layers enables untreated nylon mesh to achieve a certain level of separation efficiency when stacked in three layers because some droplets inevitably land on the stacked nylon fibers and are blocked. When the SDAP treatment time increases, even a 1-layer nylon mesh can achieve a separation efficiency of about 60%, while 2- and 3-layer stacking can reach an efficiency of over 98%.

Separation flux and recyclability are critical for evaluating the reliability of emulsion separation methods. Fig. 3c shows the flux at different stacking layers and treatment time, measured as the water flux through the mesh under unit pressure. Gravity was the driving force in this study, so the flux decreased over time. To ensure consistency, flux measurements were taken over a specific height decrease. As SDAP treatment time increased, separation flux also increased likely due to the enhanced hydrophilicity of nylon mesh. Stacking layers reduced the flux by decreasing the effective pore size, but this trade-off improved the separation efficiency. The combined effects of separation efficiency, flux, and underwater oil contact angle as a function of SDAP treatment time are shown in Fig. S9.† To assess the durability of the SDAP-treated nylon mesh, Fig. 3d shows the underwater oil contact angle and separation efficiency after multiple recycling cycles, each cycle lasting 3 hours. Even after 24 hours of continuous use, separation efficiency remained above 95%, with no significant degradation in performance. However, the upper nylon mesh (in direct contact with the emulsion) exhibited a lower underwater oil contact angle than the lower layer, suggesting that prolonged contact with the organic oil phase may lead to diffusion of hydroxyl and other oxygen-containing functional groups generated by SDAP treatment, which results in the exposure of the original amide bond or migration to the surface and a decrease in the underwater oleophobicity (Fig. S10†).

For separation efficiency under harsh conditions, as shown in Fig. 3e, the 2-layer nylon meshes treated with SDAP for 30 s maintains high separation efficiency of over 90%, and the underwater oil contact angle remains above 135° even after being soaked in pH = 2 HCl solution and pH = 12 KOH solution for 24 hours, soaked in 90 °C hot water for 10 minutes,

exposed to 365 nm ultraviolet light (200 mW cm^{-2}) for 5 minutes, and subjected to 15 cycles of tape peeling. The noticeable regression in hydrophilicity and oleophobicity after soaking in acid and alkaline solutions may be due to the small fragments containing hydrophilic functional groups detaching from the nylon fibers and dissolving in the solution under the action of strong acids and bases. Fig. S12† shows the compression resistance of the nylon mesh during emulsion separation, indicating that when subjected to 180% of the applied pressure, SDAP-treated 2-layer nylon maintained over 90% separation efficiency. Observations during testing indicated that the suction pump consistently operated with sufficient capacity redundancy, which ensured that the formation of filter cakes or partial pore blockage did not notably impact pump performance. Fig. 3f and Fig. S13† present the separation efficiency of 2-layer nylon meshes treated by SDAP for 30 s for emulsions prepared with three different oils and three different surfactants. Even for highly viscous soy oil, SDAP-treated meshes demonstrate good separation performance. To further test the applicability of SDAP-treated 2-layer nylon meshes in industrial scenarios, separation tests of emulsions consisting of diesel, mineral and crude oils, which are more viscous and difficult to separate, were also carried out, and all of them showed better separation results (Fig. S14†). Additionally, the aging performance of the SDAP-treated nylon mesh was studied. As shown in Fig. S15,† after being left in the air for 90 days, the nylon mesh exhibits no significant degradation in superhydrophilicity and underwater oleophobicity. These results indicate that the SDAP-treated nylon mesh is highly effective and durable for oil/water separation and emulsion separation, even under challenging conditions, making it a reliable choice for practical applications.

The SDAP treatment imparts superhydrophilicity to the nylon mesh, causing it to be instantly coated with an ultra-thin water film upon contact with the oil–water mixture. This results in a downward capillary force from the water inside the pores and an intrusion pressure of 0, allowing the water to spontaneously flow along the nylon fibers. Simultaneously, SDAP-treated nylon mesh exhibits underwater oleophobicity. When oil contacts the pre-wetted nylon fibers, a large underwater oil contact angle θ and a capillary force F_C opposing the intrusion are generated. Because the underwater oil contact angle for a single fiber is difficult to determine experimentally, it can be approximated using eqn (2) to calculate the underwater oil contact angle $\theta_{\text{fiber\_O/W}}$:[45]

$$\cos\theta_{\text{mesh\_O/W}} = -1 + \frac{R}{R + \frac{d}{2}}[\sin\theta_{\text{fiber\_O/W}} + (\pi - \theta_{\text{fiber\_O/W}})\cos\theta_{\text{fiber\_O/W}}], \tag{2}$$

where R is the radius of a single nylon fiber, d is the pore size of the nylon mesh, and $\cos\theta_{\text{mesh\_O/W}}$ is the underwater oil contact angle of the nylon mesh. For the 600# mesh nylon used in this experiment, R is 15 μm, and d is 10 μm. Accordingly, the maximum underwater oil contact angles for the untreated and SDAP-treated nylon fibers were calculated to

be 80° and 130°, respectively. The enhancement of underwater oleophobicity ensures that the capillary force F_C exceeds the oil intrusion pressure P_{intru}, preventing oil and emulsion droplets with diameters larger than the mesh pore size from penetrating the nylon mesh. The intrusion pressure P_{intru} can be approximated using eqn (3):[31]

$$P_{intru} = -\frac{2\gamma_{OW}\cos\theta_{fiber\_O/W}}{d_0}, \qquad (3)$$

where γ_{OW} is the oil–water interfacial tension and d_0 is the gap size between fibers. For typical oil/water systems without surfactants, according to Stokes' law, the increased intrusion pressure forces oil droplets to roll freely on the membrane or mesh surface and coalesce into larger droplets, eventually rising to the surface as a floating oil layer. However, when surfactants are present, droplets struggle to coalesce naturally. Thus, the super-wetting properties of the nylon fibers play a key role. Compared to 1-layer nylon mesh, a 2-layer stacked structure significantly reduces the effective pore size in the horizontal direction and increases the complexity of the vertical structure, thereby creating a more effective fiber-emulsion contact configuration, similar to electrospun membranes.[38]

To explain the mechanism of emulsion separation by SDAP-treated nylon meshes, Fig. 4a illustrates the process of emulsion droplet interaction with the treated nylon fibers and the subsequent formation of a filter cake. Under the combined influence of fluid pressure during separation and the interfacial tension gradient on the superhydrophilic nylon fibers, emulsion droplets from various directions impact and merge on the fiber surface, forming larger droplets. As the separation process advances, the water content decreases, and the emulsion droplet density increases, making this phenomenon more likely to occur and eventually forming a filter cake on the surface of the nylon mesh. When some of the larger coalesced droplets float upward, others become pinned onto the fiber
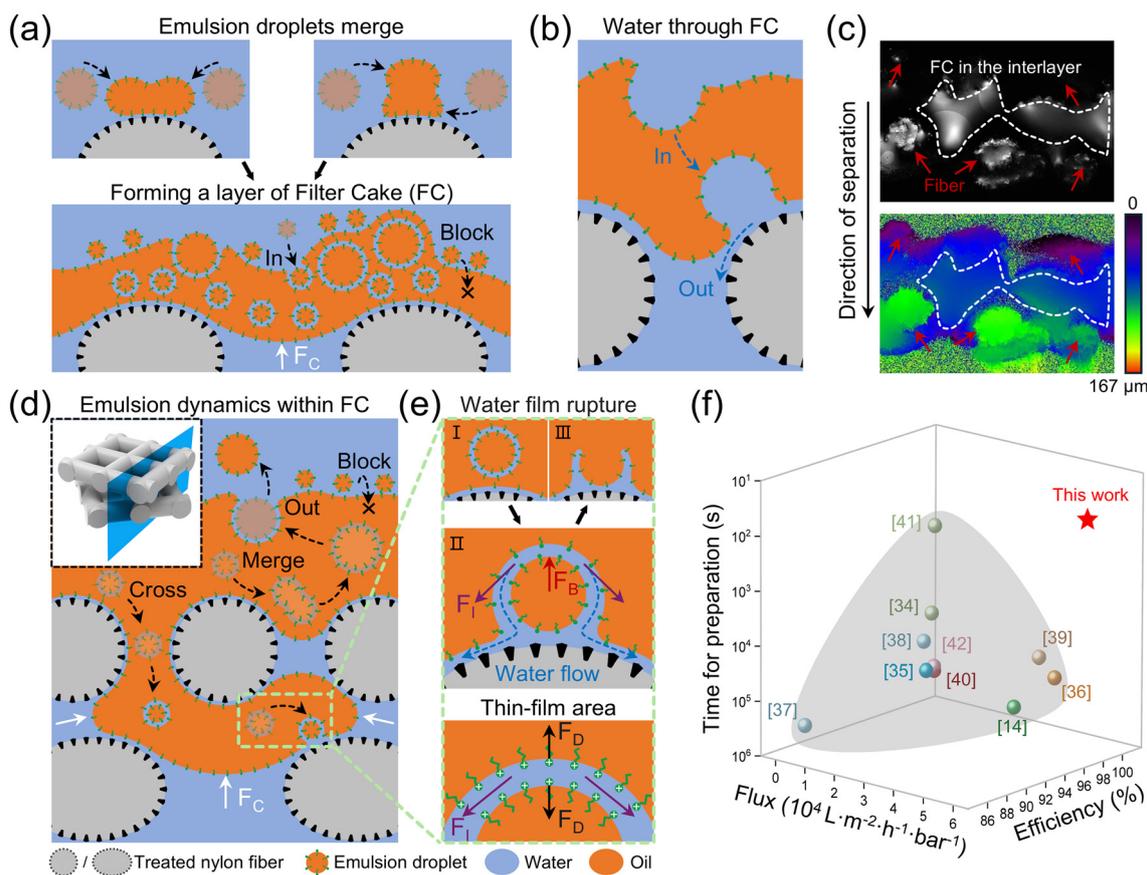
Fig. 4 Mechanism and advantage of multi-layer stacked SDAP-treated nylon meshes applied in emulsion separation. (a) and (b) Schematic of emulsion droplet merging and formation of a layer of filter cake (FC) near the treated fibers that help separation. Oil-in-water emulsion droplets enter the FC and are resisted to exit under the capillary force F_C, while few droplets are blocked (a), and water passes through the FC under gravity (b). (c) Optical microscope and laser confocal scanning microscope images show the FC in the interlayer of 2-layer stacked nylon meshes. (d) Schematic of the emulsion droplet dynamics within the FC. Inset shows that representative process occurs at the blue cross section. (e) Enlarged process of emulsion droplets demulsified when contacted by plasma-treated nylon fibers with the rupture of water film. F_I is the oil−water interfacial tension, F_B is the buoyant force and F_D is the electrostatic repulsion force between surfactant molecules at the inner and outer interfaces of the water film. (f) Comparison between this work and relevant reports[14,36−44] of membrane separation method on the time for preparation, separation flux and efficiency.

surface. The pinning occurs because the droplets, when subjected to pressure, undergo three-dimensional shape deformation on the fiber surface, causing local disruption of the water film, allowing parts of the droplet to wet the fiber surface and form pinning.[46] From this perspective, the filter cake can be observed as a byproduct of oil fouling on the nylon mesh that resembles an irregular, oversized droplet containing numerous oil-in-water-in-oil (O/W/O) droplets of varying sizes. These droplets are distributed from top to bottom under the influence of buoyancy, and as the emulsion separation process progresses, more O/W droplets are incorporated into the filter cake. However, the filter cake does not entirely block water. Due to higher density, water droplets eventually sink and either pass through the pores or, upon encountering the superhydrophilic nylon fibers, flow down along the fibers (Fig. 4b). Notably, the filter cake formation occurs not only on the upper nylon mesh surface, as shown in Fig. 4c. After achieving a separation efficiency of 98%, interlayer filter cakes were also observed using a confocal laser scanning microscope after freezing the nylon meshes in liquid nitrogen. This high separation efficiency indicates that although the filter cake blocks the pores of the nylon mesh and reduces flux, it achieves superior separation efficiency for smaller emulsions by sacrificing part of the flux.[36] The more specific mechanism can be explained as follows.

Fig. 4d presents a dynamic study of droplets within the filter cake, providing insights into the proliferation and migration of emulsion droplets. For a filter cake forming a continuous phase, the intrusion pressure can be approximated using eqn (3), revealing that filter cakes preferentially penetrate larger gaps, thereby forming interlayer filter cakes. Once the filter cake stabilizes, the original penetration pressure is decomposed into several smaller forces, offset by the reaction force provided by the fibers and the oil-resisting capillary force F_C of each gap. Consequently, a sufficient anti-penetration force continually drives O/W droplets into the filter cake, creating O/W/O droplets. Smaller droplets coalesce into larger ones due to capillary forces, eventually floating up to the surface of the filter cake or being expelled. Meanwhile, some small droplets can penetrate downward through the mesh pores of the first layer under gravity, stabilizing at a pressure equilibrium within or outside the filter cake or breaking at the superhydrophilic nylon fiber surface and merging with the filter cake, as shown in the outlined region in Fig. 4d.

The process of droplet coalescence with the filter cake upon water film rupture at the nylon fiber surface is illustrated in Fig. 4e. As the O/W/O droplets approach the nylon fibers, the oil film closest to the superhydrophilic fibers ruptures first, resulting in the formation of a three-layer structure: filter cake, water film, and droplet. In the process, oil–water interfacial tension F_I is subject to the spherical water film. Due to the interfacial tension gradient, the water film tends to shrink toward the sides, pulling away from the central area and potentially leading to localized disruptions. Meanwhile, surfactant molecules spontaneously arrange themselves at the oil–water interface typically. Taking CTAB as an example, positively charged hydrophilic groups distribute along the spherical water film interface, and repulsive force F_D between like charges prevents the water film from rupturing.[11] In this circumstance, when the interfacial tension gradient caused by the superhydrophobicity of the filter cake and the superhydrophilicity of the nylon fibers exceeds the electrostatic forces maintaining the stability of the surfactant bilayer, the water film tends to break down. This leads to droplet rupture and the subsequent merging with the filter cake, facilitating demulsification. Overall, the excellent emulsion separation performance of the multilayered nylon meshes can be attributed to two key factors: first, the reduced effective pore size in the horizontal direction due to the multilayer stacking, and second, the increased complexity of the vertical penetration structure, along with the filter cake's ability to block small droplets and the breakdown of penetration pressure by the interlayer filter cake. The results demonstrate that SDAP-treated nylon mesh achieves separation efficiency comparable to previously reported filtration materials with a higher separation flux in a shorter time (Fig. 4f and Table S4†).

Conclusions

In summary, we report a fast and green treatment of nylon mesh with super-wettability using SDAP for efficient emulsion separation. The ultra-high power density of SDAP reduces the preparation time of the super-wetting nylon mesh within 30 s and achieves superhydrophilicity and underwater oleophobicity. Meanwhile, the characterization results of SEM, AFM and XPS showed that the plasma etching effect introduced abundant hydrophilic groups and micro/nanoscale structures to the nylon fibers, which resulted in the required super-wettability. The SDAP-treated 2-layer stacked nylon meshes not only achieved high efficiency of separation for various O/W emulsions but also had good separation flux and resistance to emulsion intrusion. In addition, the treated nylon mesh has certain mechanical (resistance to tape peeling), physicochemical (resistance to acid, alkali, light, and boiling environments), and aging durability. By studying the emulsion droplet dynamics within the filter cake formed near the fibers, the mechanism behind multi-layer meshes to achieve efficient emulsion separation was first revealed, which provides insight into the research on mesh fouling issues. In practical applications, SDAP treatment demonstrates the ability to process membrane materials at a scale, facilitating the rapid preparation of large-area super-wetting nylon meshes. Coupled with the cost-effectiveness of commercially available nylon meshes and a brief treatment time, this positions SDAP technology as a highly promising candidate for industrial implementation. Overall, the SDAP technology opens the way to treat membrane materials in a wide range of filtrating, separating and screening processes because of its advantages of fast-processing, environmentally friendly, and scalable set-up.

Experimental

Materials

Nylon (polyamide-6.6) meshes with mesh numbers 600 and 150 were bought from Hebei Shanghai Bolting Cloth Manufacturing Co. (Hebei, China). 600# nylon meshes are employed for most surface characterizations and emulsion separation experiments, while 150# nylon mesh is used for capturing SEM images (Fig. 3a, inset) to observe the morphology of stacked nylon meshes. *n*-Dodecane, simethicone, hexadecyltrimethylammonium bromide (CTAB), sodium dodecyl sulfate (SDS), Tween 80, and carbon tetrachloride were purchased from Innochem. Soy oil was purchased from a local supermarket. Diesel, mineral oil and crude oil were obtained from the Research Institute of Petroleum Processing. 3 M test tape type 810 for adhesion testing was purchased from a local supermarket.

Plasma treatment

The surface diffuse atmospheric plasma (SDAP) device, which is based on a coplanar dielectric barrier discharge (CDBD) mechanism, was the same as that used in the previous study.[32] In brief, the SDAP discharging system comprises two parallel strip electrodes fixed onto an alumina ceramic substrate with a thickness of approximately 0.4 mm. The system operates under a high-frequency alternating power source, providing a voltage of 10 kV and a frequency of 20 kHz. The power supply was maintained at 100 W input power for all nylon mesh SDAP treatments, and the degree of treatment was changed only by varying the time of SDAP treatment. The nylon mesh is securely adhered to the surface of the plasma generation device to facilitate effective surface treatment. The working atmosphere of SDAP was an atmospheric environment at room temperature.

Instrument and characterization

Contact angles were measured using a contact angle system (Data-physics OCA20, Germany). For the water contact angle test in air, 3 μL of deionized water was used, and for the oil contact angle test underwater, 3 μL of ethylene dichloride was used. Microscopic images were obtained by applying a metallographic microscope (Nikon LV100ND, Japan). Scanning electron microscope (SEM) images were obtained using a field emission scanning electron microscope (HITACHI Su8010, Japan). Atomic force microscope (AFM) images were obtained by applying an atomic force microscope (Dimension FastscanBio, USA). X-ray photoelectron spectroscope (XPS) analysis was acquired with a K-Alpha spectrometer (Thermo Scientific, USA). Laser scanning confocal microscope (LSCM) images were obtained by applying a laser scanning confocal microscope (OLYMPUS OLS-4500, Japan). The oil content in the filtrate was measured by applying an infrared spectrophotometer (OIL 480, China).

Emulsion separation

SDAP-treated 2-layer stacked nylon meshes were fixed between two glass tubes with an inner diameter of 15 mm using a clamping device. Before the separation process, the treated nylon meshes were pre-wetted by water. Then, the emulsion (water : oil = 10 : 1 v/v; surfactant concentration 0.1 mg mL^{-1}) was poured into the upper tube. *n*-Dodecane, simethicone, soy oil, diesel, mineral oil and crude oil were used as different oil phases. CTAB, SDS and Tween 80 were used as different kinds of surfactant. CTAB was used as a surfactant when not explicitly stated. When not otherwise specified, the emulsions discussed were consistent with *n*-dodecane and CTAB.

Author contributions

H. D.: writing – review & editing, supervision and project administration. Z. H. (first author): coonceptualization, methodology, investigation, data curation and writing – original draft. L. Y.: data curation and writing – review & editing. X. C.: writing – review & editing. S. Z.: writing – review & editing. L. J.: writing – review & editing.

Data availability

The data supporting the findings of this study are available in the article and its ESI.†

Conflicts of interest

There are no conflicts to declare.

Acknowledgements

References

1 Y. Dong, Y. Liu, C. Hu, I. R. MacDonald and Y. Lu, *Science*, 2022, **376**, 1300–1304.
2 S. Hong, S. Bae, H. Jeon, M. Kim, S. Cho and G. Lim, *Nanoscale*, 2018, **10**, 3037–3045.
3 Z. Luo, K. Chen, J. Wang, D. Mo and S. Lyu, *J. Mater. Chem. A*, 2016, **4**, 10566–10574.
4 Y. Yan, X. Zeng, K. Yang, P. Zhou, S. Xu, P. Pi, H. Li, J. Fang, S. Wang and X. Wen, *J. Hazard. Mater.*, 2021, **418**, 126346.
5 A. Ghaffarkhah, S. A. Hashemi, A. A. Isari, M. Panahi-Sarmad, F. Jiang, T. P. Russel, O. J. Rojas and M. Arjmand, *Chem. Soc. Rev.*, 2024, **53**, 9652–9717.
6 X. Liu, S. Ni, X. Chen, Z. Li, Y. Fu, M. Qin and F. Zhang, *Green Chem.*, 2024, **26**, 3418–3428.
7 X. Wang, M. Li, Y. Shen, Y. Yang, H. Feng and J. Li, *Green Chem.*, 2019, **21**, 3190–3199.
8 W. Zhang, R. Qu, X. Li, Y. Liu, Y. Wei and L. Feng, *J. Mater. Chem. A*, 2019, **7**, 27156–27163.

9 J. Rong, F. Qiu, T. Zhang, X. Zhang, Y. Zhu, J. Xu, D. Yang and Y. Dai, *Chem. Eng. J.*, 2017, **322**, 397–407.

10 M. Arshadi, M. Azizi, H. Souzandeh, C. Tan, S. M. Davachi and A. Abbaspourrad, *J. Mater. Chem. A*, 2019, **7**, 26456–26468.

11 H. Dai, L. Yang, Y. Feng, J. Sun, F. Chen, X. Luo, Z. He, X. Xu, B. Wang, X. Liu, Z. Dong and L. Jiang, *Adv. Funct. Mater.*, 2023, **33**, 2304459.

12 Z. Liu, Z. Zhan, T. Shen, N. Li, C. Zhang, C. Yu, C. Li, Y. Si, L. Jiang and Z. Dong, *Nat. Commun.*, 2023, **14**, 4128.

13 R. K. Gupta, G. J. Dunderdale, M. W. England and A. Hozumi, *J. Mater. Chem. A*, 2017, **5**, 16025–16058.

14 J. Wu, Y. Su, Z. Cui, Y. Yu, J. Qu, J. Hu, Y. Cai, J. Li, D. Tian and Q. Zhang, *Nano Res.*, 2023, **16**, 5665–5675.

15 K. Ikigaki, K. Okada, Y. Tokudome, T. Toyao, P. Falcaro, C. J. Doonan and M. Takahashi, *Angew. Chem., Int. Ed.*, 2019, **58**, 6886–6890.

16 A. Mähringer, M. Hennemann, T. Clark, T. Bein and D. D. Medina, *Angew. Chem., Int. Ed.*, 2021, **60**, 5519–5526.

17 G. Liu, W. Jin and N. Xu, *Chem. Soc. Rev.*, 2015, **44**, 5016–5030.

18 Q. Yang, Y. Su, C. Chi, C. T. Cherian, K. Huang, V. G. Kravets, F. C. Wang, J. C. Zhang, A. Pratt, A. N. Grigorenko, F. Guinea, A. K. Geim and R. R. Nair, *Nat. Mater.*, 2017, **16**, 1198–1202.

19 F. Liu, N. A. Hashim, Y. Liu, M. R. M. Abed and K. Li, *J. Membr. Sci.*, 2011, **375**, 1–27.

20 T. A. Otitoju, A. L. Ahmad and B. S. Ooi, *J. Water Process Eng.*, 2016, **14**, 41–59.

21 Y. Wu, C. Xiao and J. Zhao, *RSC Adv.*, 2019, **9**, 33722–33732.

22 H. Liang, X. Cao, W. Zhang, H. Lin, F. Zhou, L. Chen and S. Yu, *Adv. Funct. Mater.*, 2011, **21**, 3851–3858.

23 M. Liu, S. Wang and L. Jiang, *Nat. Rev. Mater.*, 2017, **2**, 17036.

24 Z. Liu, Y. Si, C. Yu, L. Jiang and Z. Dong, *Chem. Soc. Rev.*, 2024, **53**, 10012–10043.

25 D. Hetemi and J. Pinson, *Chem. Soc. Rev.*, 2017, **46**, 5701–5713.

26 D. Li, K. Xu and Y. Zhang, *Polymer*, 2022, **14**, 3759.

27 J. Peran and S. Ercegović Ražić, *Text. Res. J.*, 2020, **90**, 1174–1197.

28 Y. Ren, L. Xu, C. Wang, X. Wang, Z. Ding and Y. Chen, *Appl. Surf. Sci.*, 2017, **426**, 612–621.

29 F. Chen, J. Song, Z. Liu, J. Liu, H. Zheng, S. Huang, J. Sun, W. Xu and X. Liu, *ACS Sustainable Chem. Eng.*, 2016, **4**, 6828–6837.

30 R. Wang, Y. Shen, C. Zhang, P. Yan and T. Shao, *Appl. Surf. Sci.*, 2016, **367**, 401–406.

31 L. Yang, Y. Feng, Z. He, X. Jiang, X. Luo, H. Dai and L. Jiang, *Nano Res.*, 2023, **16**, 9625–9632.

32 L. Yang, J. Sun, Z. He, D. Hao, Y. Feng, H. Dai and L. Jiang, *RSC Adv.*, 2024, **14**, 18073–18079.

33 S. Klébert, S. Tilajka, L. Románszki, M. Mohai, E. Csiszár and Z. Károly, *Surf. Interfaces*, 2021, **22**, 100826.

34 V. Štěpánová, P. Slavíček, M. Stupavská, J. Jurmanová and M. Černák, *Appl. Surf. Sci.*, 2015, **355**, 1037–1043.

35 M. Černák, L. Černáková, I. Hudec, D. Kováčik and A. Zahoranová, *Eur. Phys. J.:Appl. Phys.*, 2009, **47**, 22806.

36 H. Yang, J. Pi, K. Liao, H. Huang, Q. Wu, X. Huang and Z. Xu, *ACS Appl. Mater. Interfaces*, 2014, **6**, 12566–12572.

37 S. Gao, J. Chen, Y. Zheng, A. Wang, D. Dong, Y. Zhu, Y. Zhang, W. Fang and J. Jin, *Adv. Funct. Mater.*, 2022, **32**, 2205990.

38 J. Ge, D. Zong, Q. Jin, J. Yu and B. Ding, *Adv. Funct. Mater.*, 2018, **28**, 1705051.

39 Y. Gu, H. Li, L. Liu, J. Li, B. Zhang and H. Ma, *Carbon*, 2021, **178**, 678–687.

40 H. Zhang, Z. Wang, Y. Shen, P. Mu, Q. Wang and J. Li, *J. Colloid Interface Sci.*, 2020, **561**, 861–869.

41 Y. Chen, N. Wang, F. Guo, L. Hou, J. Liu, J. Liu, Y. Xu, Y. Zhao and L. Jiang, *J. Mater. Chem. A*, 2016, **4**, 12014–12019.

42 Y. He, K. Xu, X. Feng, L. Chen and Z. Jiang, *J. Membr. Sci.*, 2021, **637**, 119644.

43 J. Sun, H. Bi, S. Su, H. Jia, X. Xie and L. Sun, *J. Membr. Sci.*, 2018, **553**, 131–138.

44 Y. Wang, H. Yang, Y. Yang, L. Zhu, Z. Zeng, S. Liu, Y. Li and Z. Liang, *Sep. Purif. Technol.*, 2022, **285**, 120298.

45 P. Zhao, N. Qin, C. L. Ren and J. Z. Wen, *Appl. Surf. Sci.*, 2019, **466**, 282–288.

46 G. Fux and G. Z. Ramon, *Environ. Sci. Technol.*, 2017, **51**, 13842–13849.